Does ultrafiltration kinetics bias iron isotope compositions?

Elaheh Lotfi-Kalahroodi, Anne-Catherine Pierson-Wickmann, Olivier Rouxel, Martine Bouhnik-Le Coz, Mélanie Davranche

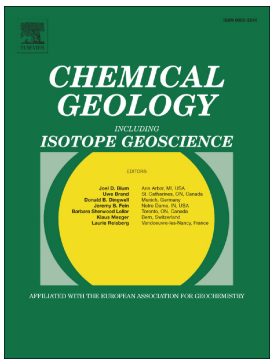

Does ultrafiltration kinetics bias iron isotope compositions?

Elaheh Lotfi-Kalahroodi, Anne-Catherine Pierson-Wickmann, Olivier Rouxel, Martine Bouhnik-Le Coz, Mélanie Davranche

PII: S0009-2541(21)00026-7

DOI: https://doi.org/10.1016/j.chemgeo.2021.120082

Reference: CHEMGE 120082

To appear in: *Chemical Geology*

Received date: 21 November 2020

Revised date: 18 January 2021

Accepted date: 21 January 2021

Please cite this article as: E. Lotfi-Kalahroodi, A.-C. Pierson-Wickmann, O. Rouxel, et al., Does ultrafiltration kinetics bias iron isotope compositions?, *Chemical Geology* (2021), https://doi.org/10.1016/j.chemgeo.2021.120082

Does ultrafiltration kinetics bias iron isotope compositions?

Elaheh Lotfi-Kalahroodi[a,1,*], Anne-Catherine Pierson-Wickmann[a], Olivier Rouxel[b], Martine Bouhnik-Le Coz[a] and Mélanie Davranche[a]

[a]Univ. Rennes, CNRS, Géosciences Rennes - UMR 6118, 35000 Rennes, France

[b]IFREMER, Unité de Géosciences Marines, 29280 Plouzané, France

For revision to Chemical geology

***Corresponding authors: elaheh.lotfi-kalahroodi@protonmail.com**

Abstract

Iron (Fe) isotopes are now recognized as useful tracers of Fe sources and biogeochemical processes in natural environments but many uncertainties remain regarding the mechanisms that control their isotopic fractionation. Ultrafiltration techniques applied to separate Fe species could potentially bias Fe isotopic compositions. Here, we investigated frontal centrifugal ultrafiltration. We have set up time-ultrafiltration experiments at low and high Fe concentrations both with and without organic matter (OM) at pH values of 1 and 6.5. The ultrafiltration impact was studied by monitoring the Fe isotope composition in the < 30 kDa ultrafiltrates relative to the ultrafiltration time. No Fe isotopes bias resulted from the ultrafiltration technique regardless the Fe and OM concentrations and speciation. This work, therefore, validates the use of the frontal centrifugal ultrafiltration technique to study the signature of Fe isotopes in environmental samples composed of various Fe species sizes such as colloids, nanoparticles, clusters or soluble complexes.

Keywords

Ultrafiltration kinetics, Speciation, Iron, Isotopic fractionation

[1] Now at : CNRS/Univ Pau & Pays Adour/ E2S UPPA, Institut des Sciences Analytiques et de Physicochimie pour l'Environnement et les Materiaux–mira, UMR5254, 64000, Pau, France

1. Introduction

Ultrafiltration is widely used in environmental studies to separate colloidal and soluble iron (Fe) species (e.g. *Wu et al., 2001; Pokrovsky and Schott, 2002; Ingri et al., 2006; Fitzsimmons et al., 2015; Fitzsimmons et al., 2017*). The separation is generally performed with a membrane that has different cut-off thresholds. The fractionation of the Fe isotopes during the flow of aqueous solution through the membranes has been debated. Some studies have highlighted the possibility of a charge build-up on the membrane surface (Wu et al., 2012), or a modification of the effective pore size of the membrane due to filter clogging (e.g. *Alekhin et al., 2010; Escoube et al., 2015*) as a potential cause of Fe isotope fractionation due to significant changes in Fe bonding. Purely diffusive processes in solution have also been shown to lead to significant isotope fractionation (*Bourg and Sposito, 2007; Richter et al., 2006*). Isotope fractionation due to the diffusion of electrolytes in a solid, porous medium is dependent for several parameters such as the concentration, temperature, and structure of the medium. *Rodushkin et al., (2004)* conclusively demonstrated that the diffusion of Fe in solution may result in significant isotopic fractionation and proposed that lighter isotopes could potentially be enriched by diffusion through, for example, biological membranes or the boundary layer surrounding reactive particles in aquatic environments. Hence, it is crucial to further assess potential Fe isotope fractionation during the ultrafiltration of natural waters.

Up to now, different filtration techniques have been applied to separate colloids from particles: i) osmosis (e.g. *Guo et al., 1996; Guo et al., 2009*), ii) dialysis (e.g. *Gimpel et al., 2003; Pokrovsky et al., 2005; Vasyukova et al., 2010; Escoube et al., 2015*), iii) tangential flow filtration (e.g. *Guéguen et al., 2002; Mulholland et al., 2015*), and iv) frontal vacuum and/ or centrifugal ultrafiltration (e.g. *Beauvois et al., 2021, 2020; Guénet et al., 2018; Ilina et al., 2013; Oleinikova et al., 2019, 2017a, 2017b; Pokrovsky et al., 2018*). *Morgan et al., (2010)* studied Fe isotopic fractionation induced by the exchange of organic ligands in Fe-organic complexes through a dialysis membrane. Because of the near quantitative transfer of the diffusing Fe-ligand complex through the membrane, these authors did not observe any Fe isotope fractionation with this dialysis technique (*Morgan et al., 2010*). In a previous work, *Mulholland et al., (2015b)* studied the impacts of tangential flow filtration on the composition of Fe isotopes in filtrates found in natural waters from the Amazon River at both the beginning and end of the ultrafiltration procedure. These authors demonstrated that membrane clogging and/or Fe adsorption on the membrane during ultrafiltration does not modify the Fe

isotope compositions (*Mulholland et al., 2015b*). The artifacts induced on the Fe isotopic signatures using frontal vacuum ultrafiltration was investigated by *Ilina et al., (2013)* on DOM rich waters. Frontal vacuum ultrafiltration was validated as a technique to separate Fe species without having an impact on the compositions of the Fe isotopes (*Ilina et al., 2013*) because of the near-complete recovery of Fe species by the cascade filtration procedure. Despite that fact that many studies have been performed on the impact of the various (ultra)filtration methods, none of them have investigated the impact of the partial recovery of Fe species on the Fe isotopic composition of the filtrate. Moreover, because of the importance of applying Fe isotopes in environmental studies as a tracer, instead of simply verifying isotopic artifacts during a large study and discussing the results in a few paragraphs, it is worth fully investigating this issue in a complete study once and for all.

We aimed to test the hypothesis that, the modification in the membrane capacity (i.e. clogging) is capable of producing significant Fe isotopic bias with preferential enrichment of the light Fe isotopes in ultrafiltrates. In this work, Fe isotopes in ultrafiltrates due to kinetic effects of UF-induced Fe(III) hydroxide precipitation was investigated. Ultrafiltration of an Fe(III) solution both with and without organic matter (OM) was performed at low and high Fe concentrations to assess the effects of Fe speciation and concentration gradients. The Fe isotope fractionation was studied by monitoring the temporal evolution of the Fe concentrations and Fe isotope composition in the ultrafiltrate (< 30 kDa fraction).

2. Materials and methods

All of the chemicals used were of analytical grade. Solutions were prepared with ultrapure 18 MΩ water (Milli-Q system, Millipore). Teflon and plastic labwares were decontaminated (i) with 10% (v/v) HNO_3 for 24 h at 45°C (ii) and then with ultrapure water for 24 h at 45°C, and (iii) finally dried at 30°C. For sample digestion and chromatographic separation, analytical grade HNO_3 and HF were purified by triple sub-boiling distillation in PFA vessels. Hydrochloric acid was purified in a PFA acid purification system (DST-1000, Savillex). All of the experiments were performed in duplicate.

2.1. Ultrafiltration experiments without organic matter

Iron(III) solutions were prepared from $Fe(NO_3)_3.9H_2O$ salt diluted to 89 µmol L^{-1} and 2.7 mmol L^{-1} of Fe. The ionic strength (IS) was fixed at 1 mmol L^{-1} with $NaNO_3$ electrolyte solution. The pH was adjusted to 1 and 6.5 using ultrapure HNO_3 or analytical grade NaOH. The pH was fixed at 6.5 to promote Fe precipitation, while a pH value of 1 was chosen to ensure that Fe remains as free species with a solvation shell. The accuracy of the pH

measurement was ± 0.04 pH unit. The solutions/suspensions were stirred for 24 h to reach a steady-state (*Catrouillet et al., 2014; Lotfi-Kalahroodi et al., 2019*). The samples were filtered through a 0.2 µm cellulose acetate membrane (Sartorius®) previously washed with ultrapure water. Sixty mL of each filtered solution/suspension was ultrafiltered at 30 kDa by centrifugation at 2790 g using Jumbosep™ systems (Pall Laboratory). The 30 kDa ultrafiltration membrane was previously cleaned using 0.1 mol L^{-1} of NaOH and ultrapure water. Centrifugation was performed during 3 (the lowest time for the centrifuge to reach 2790 g), 4, 5, 6, 7, and 10 min to investigate the effect of time on the Fe isotopic composition of the ultrafiltered solutions. A different ultrafiltration unit was dedicated for each ultrafiltration time, and was filled with the same initial solution during each replicate. At each time, the ultrafiltrate was collected to determine its volume. The iron isotopic ratio (δ^{56}Fe and δ^{57}Fe, Table S1) and Fe concentrations were analyzed for the initial solution (total sample) and the < 30 kDa fractions for each centrifugation time. Because the small volume (dead volume >3 mL) remained in the ultrafiltration apparatus, real percentage of precipitated Fe (mol./mol.) was calculated for samples which was presented as $Fe_{\text{real precipitated}}$ % in Tables 1, 2, and 3. Real percentage of precipitated Fe at > 30 kDa for the sample i was calculated as:

$$Fe_{i\ at>30\ kDa}(mol./mol.,\%) = \left(\frac{Fe_{total} - Fe_{i\ at<30\ kDa} - ([Fe_{total}]V_{dead})}{Fe_{total}}\right) \times 100 \qquad \text{(Eq. 1)}$$

Where Fe_{total}, $Fe_{i\ at<30\ kDa}$, $[Fe_{total}]$, and V_{dead} present the amount of Fe (mol.) in the initial solution, and in the < 30 kDa filtrate for sample i, Fe concentration in the initial solution, and the dead volume remained in apparatus, respectively. The procedural blank for the (ultra)filtration membranes was assessed by processing ultrapure water throughout the entire filtration and ultrafiltration steps; the Fe concentrations were not significant (< 2 nmol L^{-1}) and never exceeded 1% of the minimum amount of Fe processed throughout the experiment. This experiment was performed for two Fe concentrations in order to be able to quantify the Fe concentration in the filtrates even at pH > 6.5.

2.2. Ultrafiltration experiments with organic matter

The OM stock solution was produced by dissolving 2 g of Gascoyne Leonardite soil (Cat. No. BS104L) obtained from the International Humic Substances Society (IHSS) (C = 49.2%, H = 4.5% and N = 0.9% as a mass fraction) in ultrapure water. Approximately 1 L of OM solution at 4.2 mmol L^{-1} of dissolved organic carbon (DOC) was titrated with Fe(III) using a $Fe(NO_3)_3$ solution at 36 mmol L^{-1} using an automated titrator (Titrino 794, Metrohm) with a target Fe/C_{org} = 0.02 (mol./mol.) (*Lotfi-Kalahroodi et al., 2019*). The solution flow was

fixed at 0.05 mL min^{-1}. A second titrator (Titrino 794, Metrohm) was used in pH mode using a NaOH solution at 100 mmol L^{-1} to fix the pH at 6.5 and provided the OH^- necessary for the hydrolysis of Fe (*Guénet et al., 2017; Lotfi-Kalahroodi et al., 2019*). After 24 h of agitation, the solution/suspension was filtered at 0.2 µm. The protocol is the same as for the experiment without OM (section 2.1). The DOC concentrations were determined for the initial solution and the < 30 kDa fractions.

2.3. Chemical analyses

The DOC concentration was analyzed using a total carbon analyzer (Shimadzu TOC-V CSH) with an uncertainty of 5% using a standard solution of potassium hydrogen phthalate (Sigma Aldrich). For the major and trace element analyses, the samples were acidified with 0.37 mol L^{-1} HNO_3. The initial solution and ultrafiltered samples containing OM were evaporated and pre-digested twice with 14.6 mol L^{-1} distilled HNO_3 at 90°C to release Fe from the organic complexes. The second step of digestion was performed using a mixture of 1 mL of 30% H_2O_2 and 2 mL of 14.6 mol L^{-1} HNO_3 to eliminate the OM. After total evaporation, they were then dissolved in 0.37 mol L^{-1} HNO_3. The Fe concentration analysis was determined using an Agilent 7700X inductively coupled plasma mass spectrometer (ICP-MS) at Geosciences Rennes (University of Rennes) with a precision of 3% and 5% for > and < 1.8 µmol L^{-1} of Fe, respectively.

2.4. Iron purification and iron isotopic measurements

The Fe isotopic composition ($\delta^{56}Fe$ and $\delta^{57}Fe$) measurement procedure was previously described in *Lotfi-Kalahroodi et al., (2019)*. In short, acidified samples were digested using a mixture of 22.6 mol L^{-1} HF and 14.6 mol L^{-1} HNO_3, then 12 mol L^{-1} HCl and 14.6 mol L^{-1} HNO_3 and finally supra pure 30% H_2O_2 and 14.6 mol L^{-1} HNO_3. After evaporating the sample to dryness on a hot plate at 90°C, the Fe was purified using the anion exchange resin Dowex® 1X8, chloride form (100-200 mesh). The purified Fe solution was evaporated to dryness at 80°C and the residue was dissolved in 0.28 mol L^{-1} of HNO_3 to measure the Fe isotope compositions using a Thermo Neptune-plus multicollector inductively coupled plasma mass spectrometer (MC-ICP-MS) in high or medium mass resolution at the French Research Institute for Exploitation of the Sea (IFREMER). The cups were set up to measure ^{52}Cr, ^{54}Fe, ^{56}Fe, ^{57}Fe, ^{58}Fe, ^{60}Ni, ^{61}Ni, and ^{62}Ni. Consequently, the interference of ^{54}Cr on ^{54}Fe was corrected using the ^{52}Cr abundances. The $^{62}Ni/^{60}Ni$ ratio measurement allowed to correct the instrumental mass bias. The isotopic data are reported in delta notation relative to the IRMM-

014 standard, expressed as δ^{56}Fe, which represents the deviation in per mil relative to the reference material:

$$\delta^{56}Fe(‰) = \left(\frac{\left({}^{56}Fe/_{54}Fe\right)_{sample}}{\left({}^{56}Fe/_{54}Fe\right)_{IRMM-014}} - 1 \right) \times 1000 \qquad \text{(Eq. 2)}$$

We introduce additional notation (δ^{56}Fe') which corresponds to the Fe isotope composition of the < 30 kDa fractions ($\delta^{56}Fe_{<30kDa}$) relative to the Fe isotope composition of the initial solution ($\delta^{56}Fe_{Total}$), such as:

$$\delta^{56}Fe'_{<30\text{kDa}}\ (‰) = \delta^{56}Fe_{<30\text{kDa}} - \delta^{56}Fe_{Total} \qquad \text{(Eq.3)}$$

The external precisions of the δ^{56}Fe values were calculated for each analytical run using the repeated measurement of the IRMM-014 and were within the range from 0.08‰ to 0.13‰ (at 2 standard deviation, 2SD). For the samples (i.e. sample A) that were analyzed twice, the mean values of the duplicate analyses are reported with their 95% confidence interval (Supplementary file Table S2 and Table S3). If two measured values for sample A are reported as $\delta^{56}Fe_1 \pm 2SD_1$ and $\delta^{56}Fe_2 \pm 2SD_2$, the error propagation of sample A would be calculated in three steps: i) determination of a minimum between reported analytical precisions, meaning $2SD_1$ and $2SD_2$; ii) calculation of 2-fold standard deviation on the two measured δ^{56}Fe values obtained by twice analyses then iii) determination a maximum value between these last two calculated values:

$$Error\ propagation\ _{\delta^{56}Fe_A} = max(\min(2SD_1, 2SD_2),\ 2\ SD\ (\delta^{56}Fe_1, \delta^{56}Fe_2)\ ) \text{ (Eq.4)}$$

The average of the experimental duplicate samples was reported as the Fe isotopic composition of each sample. The 2-fold standard deviation (2SD) of the corrected Fe isotope composition (δ^{56}Fe', Eq.3) is calculated as:

$$2SD_{\Delta^{56}Fe_{i-n}} = \sqrt{\sum_i^n (2SD_i)^2} \qquad \text{(Eq.5)}$$

Procedural blanks, including evaporation/digestion and ion exchange purification steps, were determined for each experiment. The average values of these Fe blanks are 0.43 ± 0.4 nmol, representing less than 1% of the Fe processed through purification within the range of 89.5 nmol to 1.6 µmol, and therefore these values are negligible. An internal standard BHVO-1 (a Hawaiian basalt) with an average Fe isotopic composition of δ^{56}Fe of 0.08 ± 0.13‰ (2SD, n = 10) was used to evaluate the accuracy of the method.

3. Results

3.1. Organic matter-free experiment

3.1.1. Low iron concentration experiment

At pH 1, between 3 and 10 min of ultrafiltration, the volumes of the < 30 kDa fractions varied from 49 ± 5 mL to 57 ± 9 mL (Table 1) corresponding to 82% and 95% ($V/V_{initial}$) of the initial volume, respectively. The iron concentration varied insignificantly from 79 µmol L^{-1} to 84 µmol L^{-1} which is identical, within uncertainty, to the initial Fe concentration (85 ± 4 µmol.L^{-1}, Fig. 1a and Table 1). Note that the transfer of Fe through the membrane was not quantitative (79% (mol./mol.) to 89% of the initial Fe), because the small volume remained in the ultrafiltration apparatus. The $\delta^{56}Fe_{<30kDa}$ value varied from 0.54 ± 0.14‰ (2SD) to 0.62 ± 0.13‰ (2SD) (Fig. 1b, Table 1 and in the supplementary data, Table S1) which is identical, within uncertainty, to the δ^{56}Fe of the initial solution of 0.60 ± 0.13‰. The data presents an average of $\delta^{57}Fe/\delta^{56}Fe$ at 1.40± 0.11.

At pH 6.5, the volume of the < 30 kDa fractions progressively increased from 40 mL to 54 mL, corresponding to 67% and 90% ($V/V_{initial}$) of the initial volume, respectively (Table S1). However, Fe concentrations in the < 30 kDa fractions were found below the detection limit (< 12 nmol L^{-1}). Hence, Fe quantitatively remained in the > 30 kDa fraction. The negligible amount of Fe in the < 30 kDa fractions did not allow to determine the Fe isotope composition.

3.1.2. High iron concentration experiment

Similar to the low Fe concentration experiment, from 77% to 95% of the initial volume was recovered in the < 30 kDa fractions at pH 1 (Table 2). The Fe concentration varied between 2.3 mmol L^{-1} and 2.4 mmol L^{-1} which was identical, within uncertainty, to the Fe concentration in the initial solution (2.5 ± 0.1 mmol.L^{-1}). Hence, the recovery of Fe in the filtrate increased from 76% to 91% with increasing filtration time (Fig. 1a and Table 2). The δ^{56}Fe of the < 30 kDa fractions varied from 0.54 ± 0.09‰ (2SD) to 0.63 ± 0.06‰ (2SD) (Fig. 1b, Table 2), similar to 0.57 ± 0.13‰ for the initial solution. Therefore, no isotopic variation was observed, which is similar to the low Fe concentration experiment, but higher mass-dependency $\delta^{57}Fe/\delta^{56}Fe$ ratio at 1.40 ± 0.18.

At pH 6.5, the volume of the < 30 kDa fractions varied from 43 mL to 55 mL, representing between 72% and 92% of the initial volume after 3 to 10 min of ultrafiltration (Table S2). Unfortunately, similar to the low Fe experiment, Fe mainly occurred in the > 30 kDa fractions despite a high Fe concentration in the initial solution. In the < 30 kDa fractions,

Fe represents less than 0.01% of the initial Fe. The isotopic analysis could not be performed due to too low Fe concentrations in the < 30 kDa fractions ([Fe] < 12 nmol L^{-1}). Hence, under these experimental conditions, Fe precipitated entirely in the > 30 kDa fraction. The δ^{56}Fe of the initial solution was 0.55 ± 0.13‰, which is similar to the value found at pH 1 (Table S2) and similar to the Fe low concentration experiment.

3.2. Experiment with organic matter

For the Fe-OM experiment at pH 6.5, the volume of the < 30 kDa fractions progressively increased from 33 mL to 48 mL, between 3 to 10 min of ultrafiltration, corresponding to between 55% and 80% of the initial volume passing through the 30 kDa membranes. The Fe and DOC concentrations in the < 30 kDa fractions decreased from 4.1 µmol L^{-1} and 1.07 mmol L^{-1} after 3 min to 2.2 µmol L^{-1} and 0.85 mmol L^{-1} after 10 min of ultrafiltration, respectively (Figs. 2a, 2b and Table 3). Compared to the initial Fe concentration of 104 µmol L^{-1}, this only represents a small fraction of the initial Fe pool (2.2% to 1.7%, respectively). Also, less than 17 % of OM were found in the < 30 kDa fractions. However, the Fe concentration decreased by 53% from 3 to 10 min of ultrafiltration in the < 30 kDa fractions. In the < 30 kDa fractions, the δ^{56}Fe ranged from 0.77 ± 0.13‰ to 0.87 ± 0.04‰ (Fig. 2b and Table 3) which are identical within uncertainty to each other but significantly different from that of the initial solution (0.54 ± 0.08‰). These results showed enrichment in heavy Fe isotopes in the Fe-OM complexes, with a δ^{56}Fe' ranging from 0.23 ± 0.10‰ to 0.33 ± 0.09‰ (Table 3), and a mass-dependency average (δ^{57}Fe/δ^{56}Fe) at 1.48 ± 0.07.

4. Discussion

As a previous work showed no variation in Fe isotopic compositions of the < 0.2 µm fractions compared to the initial solution for the experiments with and without OM at pH 1 and pH 6.5 (*Lotfi-Kalahroodi et al., 2019*), the first step of filtration at 0.2 µm cannot bias the Fe isotopic compositions in this work. For the low and high Fe concentration experiments at pH 1, the Fe concentration and recovered volume varied only slightly with filtration time, averaging 80 ± 8 µmol.L^{-1}, and 2.4 ± 0.1 mmol.L^{-1}, respectively, indicating that the solution was homogenously recovered with increasing ultrafiltration time. The main volume was recovered only after 3 min (Tables 1, 2, and Fig. 1a). The results showed that almost 80% of the solution passed through the membrane with 20% of the solution remaining in the supernatant or in the dead volume. The calculation of the actual amount of Fe precipitated at the > 30 kDa fractions revealed that although Fe was mainly present as an ionic free species,

at pH 1, approximately 20% of the Fe remained in the > 30 kDa fractions, which contained 2% and 0.4% of the precipitated or polymeric Fe(III) ($Fe_{\text{real precipitated}}$ % in Table 1 and Table 2) respectively, after 3 min of frontal centrifugal ultrafiltration. In these experiments, the Fe precipitated varied from 2 to 8%, and 0.4 to 4.4%, respectively (Tables 1 and 2). The lack of significant variation in $\delta^{56}Fe$ demonstrated that ultrafiltration does not fractionate the Fe isotopes with the ultrafiltration time (Supplementary data, Table S1). Our previous work demonstrated a precipitation rate of 7% of Fe in the > 30 kDa fraction at pH 1, but despite this Fe precipitation, the Fe isotopic ratios varied weakly within a similar range from 0.50 ± 0.05‰ for complete ultrafiltration at 30 kDa to 0.57 ± 0.05‰ for the initial Fe solution, and therefore, no Fe isotopic fractionation occurred (*Lotfi-Kalahroodi et al., 2019*). The $\delta^{57}Fe/\delta^{56}Fe$ averages at 1.40 ± 0.11 and 1.40 ± 0.18 for low and high Fe concentration experiments confirmed the mass dependency of Fe isotopes. However, frontal centrifugal ultrafiltration at pH 1 either does not involve the fractionation of Fe isotopes or this fractionation occurs within the first minutes of the ultrafiltration (< 3 min). The early fractionation is then compensated with the ultrafiltration time. In general, diffusion-driven isotopic fractionation is experimentally assessed by putting together two phases with contrasted compositions. The lighter isotopes diffuse faster than the heavier ones, such that in diffusive processes, the source reservoir gets enriched in the heavier isotopes while the sink reservoir gets enriched in the lighter isotopes. The reason why diffusion-driven isotopic fractionation is expected to be extremely small is that Fe does not diffuse as free ions because Fe is surrounded by a large solvation shell, the difference in mass of the effective diffusing molecule must be therefore small when Fe isotopes are substituted (*Dauphas et al., 2017*). The flux of component i in a n-component system is defined by its diffusion coefficient D_i from Fick's law (*Joesten, 1991*):

$$J_i = -D_i \frac{\partial C_i}{\partial X} \quad \text{(Eq. 6)}$$

J_i, Ci, and X represent the diffusion flux, concentration of component i and distance, respectively. The calculation of the diffusion constant through Fick's law (when J_i=0)showed that the diffusion coefficient was negligible at 3 min ($D_{low} = 6 \times 10^{-6}\ m^2\ S^{-1}$ and $D_{high} = 3 \times 10^{-5}\ m^2\ S^{-1}$). However, during the frontal centrifugal ultrafiltration, filtration is performed via the pressure exerted by the centrifugation and this system therefore excluded diffusion. No ultrafiltration kinetic effect was observed on the Fe isotopic signature at pH 1. At pH 6.5, regardless of the Fe concentration in the initial solution, 0.01% of the Fe was recovered in the < 30 kDa fractions and Fe then occurred in the > 30 kDa fraction. Kinetic fractionation of Fe

isotopes was reported in several studies due to partial precipitation of Fe-containing minerals under specific conditions such as pH <3 (*Balci et al., 2006*), high temperature (100°C, *Guilbaud et al., 2011)*, biotic processes (*Kappler et al., 2010; Swanner et al., 2017, 2015*). Although *Skulan et al., (2002)* observed kinetic Fe fractionation during rapid hematite precipitation, they reported insignificant Fe fractionation for slow precipitation of Fe. In our previous work, we demonstrated that the abiotic precipitation of amorphous Fe oxyhydroxides does not fractionate Fe isotopes between the Fe precipitates and dissolved Fe fractions (*Lotfi-Kalahroodi et al., 2019*).

As measured and reported in a previous work (*Lotfi-Kalahroodi et al., 2019*), the initial OM used in the Fe-OM experiment contained 9% of the total Fe, with a δ^{56}Fe of 0.09 ± 0.04‰. The impact of the Fe impurities on the δ^{56}Fe of the initial solution was negligible and close to the analytical uncertainty. Therefore, no specific correction was needed in δ^{56}Fe. For the Fe-OM experiment, the Fe and DOC concentrations varied significantly with time. The results showed that with increasing ultrafiltration time, the Fe concentration decreased by more than 53% (4.1 to 2.2 µmol L^{-1}), while the volume increased by 69% (33 to 48 mL) indicating a significant decrease in the amount of Fe through the progressive precipitation of Fe hydroxides on the membrane over time. According to the calculation, between 53% and 78% of the total Fe precipitated from 3 min to 10 min of ultrafiltration ($Fe_{\text{real precipitated}}$ % in Table 3). This suggested that the capacity of the membrane therefore evolved with the ultrafiltration time. The δ^{56}Fe of the < 30 kDa fractions were higher than the δ^{56}Fe of the initial solution, with $\delta^{56}Fe'_{<30\ kDa\text{-}total}$ varying from 0.23 ± 0.10‰ to 0.33 ± 0.09‰ (Fig. 2b and Table 3). Despite the enrichment of the < 30 kDa fractions in heavy Fe isotopes compared to the initial solution (Table 3), the modification in the membrane capacity over time (i.e. clogging) did not show any significant change in Fe isotopic fractionation. The increase of δ^{56}Fe in the < 30 kDa fractions is explained by the binding of Fe with OM occurring at pH 6.5. According to several authors (*Conway and John, 2014; Dideriksen et al., 2008; Ilina et al., 2013; Lotfi-Kalahroodi et al., 2019; Morgan et al., 2010*), complexation between Fe and strong organic ligands promotes heavy Fe isotopes due to strong Fe-OM bindings. The magnitude of the Fe isotopic fractionation produced by Fe-OM complexation was in the range of 0.3 to 0.7‰ (*Conway and John, 2014; Lotfi-Kalahroodi et al., 2019*). Our results revealed the mass-dependent fractionation of Fe isotopes with an average $\delta^{57}Fe/\delta^{56}Fe$ at 1.48 ± 0.07.What is more interesting in the present work is that, despite the binding of Fe to OM and the enrichment of heavy Fe isotopes in the < 30 kDa fraction, no significant δ^{56}Fe variations were observed with time (i.e. from 3 to 10 min). Despite the strong evolution in terms of the

efficiency of the membrane to separate Fe-OM complexes, no effect due to membrane clogging was observed on the Fe isotope compositions with the ultrafiltration time (from 3 to 10 min).

As mentioned above, *Morgan et al. (2010)* measured the equilibrium isotope fractionation during organic ligand exchanges between Fe(III)-desferrioxamine B (DFOB) and (i) Fe(III)-oxalate and (ii) Fe(III)-ethylenediaminetetraacetic acid (EDTA) through a dialysis membrane. The separation was performed after equilibration of the Fe-ligand pools by trapping Fe(III)-DFOB and diffusing both the Fe(III)-oxalate and Fe(III)-EDTA complexes through the dialysis membrane. The results showed an Fe isotopic fractionation between the Fe(III)-DFOB and Fe-oxalate complexes of Δ^{56}Fe$_{(Fe\text{-}DFOB)\text{-}(Fe\text{-}oxalate)}$ = 0.20 ± 0.11‰ whereas the isotopic fractionation between Fe(III) DFOB and Fe(III)-EDTA was insignificant (*Morgan et al., 2010*). Their study revealed that despite the diffusion occurring for the separation of the Fe complexes, Fe isotopes do not fractionate. Moreover, *Gangloff, (2016)* verified the potential fractionation of the calcium (Ca) and strontium (Sr) isotopes during the tangential flow filtration. They observed the identical $\delta^{44/40}$Ca and insignificant variations in the ^{87}Sr/^{86}Sr ratio for the various filtered and ultrafiltered fractions.

Therefore, we infer that frontal centrifugal ultrafiltration does not produce any Fe isotopic artifacts. As a result, the observed Fe isotope fractionation cannot be a result of ultrafiltration kinetic artifacts or clogging effects induced by the membrane. It should be distinguished the various processes that can affect the Fe isotopic composition: (1) water storage conditions from field to the laboratory (*Mulholland et al., 2015a*); (2) diffusion of aqueous chemical species (*Richter et al., 2006*) (3) chemical interactions with the membrane and/or container; (4) modification of the speciation in the retentate (removing the chemical species that passes through the membrane will in turn modify the chemical equilibrium and the redistribution of the species/isotopes); (5) evolution of the capacity of the membrane over time (e.g. clogging); and (6) particular operating problems, e.g. in suboxic and anoxic environments, O_2 and UV may modify the Fe isotopic signature of the samples during ultrafiltration if it is not performed under an anoxic atmosphere. Ultrafiltration is therefore a powerful tool to study the distribution of Fe-OM particles, colloids, and free species in environmental systems and Fe isotopes are valuable tracers to study biogeochemical mechanisms produced under environmental conditions.

5. Conclusion

This work focused on the potential impact and kinetic effect of frontal centrifugal ultrafiltration by monitoring the temporal evolution of the Fe isotope compositions. The isotopic data analysis did not demonstrate any bias of the Fe isotopes with the ultrafiltration time for the low and high concentrations of Fe with and without natural DOM (Fe/C_{org} = 0.02 (mol./mol.)). The present results confirmed that ultrafiltration either does not impact on the compositions of the Fe isotopes or, if it does, this impact rapidly disappears, within the first minutes of the ultrafiltration (< 3 min). As a result, this study highlights the usefulness and importance of ultrafiltration in studies on the speciation of natural and/or experimental Fe-OM particles, colloids, and soluble species without any bias on isotopic results.

Acknowledgements

This work was supported by the ISO-TRANS-FER project funded by INSU EC2CO program. Through the support of the GeOHeLiS analytical platform at Rennes University, this publication is also supported by the European Union through the European Regional Development Fund (FEDER), the French Ministry of Higher Education and Research, the French Region of Brittany, and Rennes Metropole. The authors would like to thank Dr. Oleg Pokrovsky, Dr. Franck Poitrasson, and the anonymous reviewer for their help and advice.

REFERENCES

Alekhin, Y. V., Ilina, S.M., Lapitskiy, S A., Sitnikova, M. V., 2010. Results of a study of co-migration of trace elements and organic matter in a river flow in a boreal zone. Moscow University Geology Bulletin 65, 380–386. https://doi.org/10.3103/s0145875210060050

Balci, N., Bullen, T.D., Witte-Lien, K., Shanks, W.C., Motelica, M., Mandernack, K.W., 2006. Iron isotope fractionation during microbially stimulated Fe(II) oxidation and Fe(III) precipitation. Geochimica et Cosmochimica Acta 63, 113–127. https://doi.org/10.1016/j.gca.2005.09.025

Beauvois, A., Vantelon, D., Jestin, J., Bouhnik-Le Coz, M., Catrouillet, C., Briois, V., Bizien, T., Davranche, M., 2021. How crucial is the impact of calcium on the reactivity of iron-organic matter aggregates? Insights from arsenic. Journal of Hazardous Materials 404, 124127. https://doi.org/10.1016/j.jhazmat.2020.124127

Beauvois, A., Vantelon, D., Jestin, J., Rivard, C., Bouhnik-Le Coz, M., Dupont, A., Briois, V., Bizien, T., Sorrentino, A., Wu, B., Appavou, M.S., Lotfi-Kalahroodi, E., Pierson-Wickmann, A.C., Davranche, M., 2020. How does calcium drive the structural organization of iron-organic matter aggregates? A multiscale investigation. Environmental Science: Nano 7, 2833. https://doi.org/10.1039/d0en00412j

Benoit, G., Rozan, T.F., 1999. The influence of size distribution on the particle concentration effect and trace metal partitioning in rivers. Geochimica et Cosmochimica Acta 63, 113–127. https://doi.org/10.1016/S0016-7037(98)00276-2

Bourg, I.C., Sposito, G., 2007. Molecular dynamics simulations of kinetic isotope

fractionation during the diffusion of ionic species in liquid water. Geochimica et Cosmochimica Acta 71, 5583–5589. https://doi.org/10.1016/j.gca.2007.01.021

Catrouillet, C., Davranche, M., Dia, A., Bouhnik-Le Coz, M., Marsac, R., Pourret, O., Gruau, G., 2014. Geochemical modeling of Fe(II) binding to humic and fulvic acids. Chemical Geology 372, 109–118. https://doi.org/10.1016/j.chemgeo.2014.02.019

Conway, T.M., John, S.G., 2014. Quantification of dissolved iron sources to the North Atlantic Ocean. Nature 511, 212–215.

Dauphas, N., John, S.G., Rouxel, O., 2017. Iron Isotope Systematics. Reviews in Mineralogy and Geochemistry 82, 415–510. https://doi.org/10.2138/rmg.2017.82.11

Dideriksen, K., Baker, J.A., Stipp, S.L.S., 2008. Equilibrium Fe isotope fractionation between inorganic aqueous Fe(III) and the siderophore complex, Fe(III)-desferrioxamine B. Earth and Planetary Science Letters 269, 280–290. https://doi.org/10.1016/j.epsl.2008.02.022

Dupré, B., Viers, J., Dandurand, J.-L., Polve, M., Bénézeth, P., Vervier, P., Braun, J.-J., 1999. Major and trace elements associated with colloids in organic-rich river waters: ultrafiltration of natural and spiked solutions. Chemical Geology 160, 63–80. https://doi.org/10.1016/S0009-2541(99)00060-1

Escoube, R., Rouxel, O.J., Pokrovsky, O.S., Schroth, A., Max Holmes, R., Donard, O.F.X., 2015. Iron isotope systematics in Arctic rivers. Comptes Rendus - Geoscience 347, 377–385. https://doi.org/10.1016/j.crte.2015.04.003

Fitzsimmons, J.N., Carrasco, G.G., Wu, J., Roshan, S., Hatta, M., Measures, C.I., Conway, T.M., John, S.G., Boyle, E.A., 2015. Partitioning of dissolved iron and iron isotopes into soluble and colloidal phases along the GA03 GEOTRACES North Atlantic Transect. Deep Sea Research Part II: Topical Studies in Oceanography, GEOTRACES GA-03 - The U.S. GEOTRACES North Atlantic Transect 116, 130–151. https://doi.org/10.1016/j.dsr2.2014.11.014

Fitzsimmons, J.N., John, S.G., Marsay, C.M., Hoffman, C.L., Nicholas, S.L., Toner, B.M., German, C.R., Sherrell, R.M., 2017. Iron persistence in a distal hydrothermal plume supported by dissolved–particulate exchange. Nature Geoscience 10, 195–201. https://doi.org/10.1038/ngeo2900

Gangloff, S.L., 2016. Evaluation of the mechanisms of trace elements transport (Pb, Rare Earth Elements,...) and the elemental and isotopic fractionation (Ca and Sr) at the interface water-soil-plant. Université de Strasbourg.

Gimpel, J., Zhang, H., Davison, W., Edwards, A.C., 2003. In situ trace metal speciation in lake surface waters using DGT, dialysis, and filtration. Environmental Science and Technology 37, 138–146. https://doi.org/10.1021/es0200995

Guéguen, C., Belin, C., Dominik, J., 2002. Organic colloid separation in contrasting aquatic environments with tangential flow filtration. Water Research 36, 1677–1684. https://doi.org/10.1016/S0043-1354(01)00374-8

Guénet, H., Davranche, M., Vantelon, D., Gigault, J., Prévost, S., Taché, O., Jaksch, S., Pédrot, M., Dorcet, V., Boutier, A., 2017. Characterization of iron–organic matter nano-aggregate networks through a combination of SAXS/SANS and XAS analyses: impact on As binding. Environmental Science: Nano 4, 938–954.

Guénet, H., Demangeat, E., Davranche, M., Vantelon, D., Pierson-Wickmann, A.-C., Jardé,

E., Bouhnik-Le Coz, M., Lotfi, E., Dia, A., Jestin, J., 2018. Experimental evidence of REE size fraction redistribution during redox variation in wetland soil. Science of the Total Environment 631–632, 580–588. https://doi.org/10.1016/j.scitotenv.2018.03.005

Guilbaud, R., Butler, I.B., Ellam, R.M., 2011. Abiotic Pyrite Formation Produces a Large Fe Isotope Fractionation. Science 332, 1548–1551. https://doi.org/10.1126/science.1202924

Guo, L., Santschi, P.H., Cifuentes, L.A., Trumbore, S.E., Southon, J., 1996. Cycling of high-molecular-weight dissolved organic matter in the Middle Atlantic Bight as revealed by carbon isotopic (13C and 14C) signatures. Limnology and Oceanography 41, 1242–1252. https://doi.org/10.4319/lo.1996.41.6.1242

Guo, L., White, D.M., Xu, C., Santschi, P.H., 2009. Chemical and isotopic composition of high-molecular-weight dissolved organic matter from the Mississippi River plume. Marine Chemistry 41, 1242–1252. https://doi.org/10.1016/j.marchem.2009.04.002

Ilina, S.M., Drozdova, O.Y., Lapitskiy, S.A., Alekhin, Y. V., Demin, V. V., Zavgorodnyaya, Y.A., Shirokova, L.S., Viers, J., Pokrovsky, O.S., 2014. Size fractionation and optical properties of dissolved organic matter in the continuum soil solution-bog-river and terminal lake of a boreal watershed. Organic Geochemistry 66, 14–24. https://doi.org/10.1016/J.ORGGEOCHEM.2013.10.003

Ilina, S.M., Poitrasson, F., Lapitskiy, S.A., Alekhin, Y. V., Viers, J., Pokrovsky, O.S., 2013. Extreme iron isotope fractionation between colloids and particles of boreal and temperate organic-rich waters. Geochimica et Cosmochimica Acta 101, 96–111. https://doi.org/10.1016/j.gca.2012.10.023

Ingri, J., Malinovsky, D., Rodushkin, I., Baxter, D.C., Widerlund, A., Andersson, P., Gustafsson, Ö., Forsling, W., Öhlander, B., 2006. Iron isotope fractionation in river colloidal matter. Earth and Planetary Science Letters 245, 792–798. https://doi.org/10.1016/j.epsl.2006.03.031

Joesten, R., 1991. Diffusion, atomic ordering, and mass transport. Edited by Ganguly J. New York: Springer-Verlag 343–395.

Kappler, A., Johnson, C.M., Crosby, H.A., Beard, B.L., Newman, D.K., 2010. Evidence for equilibrium iron isotope fractionation by nitrate-reducing iron(II)-oxidizing bacteria. Geochimica et Cosmochimica Acta 74, 2826–2842. https://doi.org/https://doi.org/10.1016/j.gca.2010.02.017

Lotfi-Kalahroodi, E., Pierson-Wickmann, A.-C., Guénet, H., Rouxel, O., Ponzevera, E., Bouhnik-Le Coz, M., Vantelon, D., Dia, A., Davranche, M., 2019. Iron isotope fractionation in iron-organic matter associations: Experimental evidence using filtration and ultrafiltration. Geochimica et Cosmochimica Acta 250, 98–116. https://doi.org/10.1016/j.gca.2019.01.036

Morgan, J.L.L., Wasylenki, L.E., Nuester, J., Anbar, A.D., 2010. Fe isotope fractionation during equilibration of Fe-organic complexes. Environmental Science and Technology 44, 6095–6101. https://doi.org/10.1021/es100906z

Mulholland, Daniel S., Poitrasson, F., Boaventura, G.R., 2015. Effects of different water storage procedures on the dissolved Fe concentration and isotopic composition of chemically contrasted waters from the Amazon River Basin. Rapid Communications in Mass Spectrometry 29 (21), 2102-2108. https://doi.org/10.1002/rcm.7368

Mulholland, Daniel Santos, Poitrasson, F., Boaventura, G.R., Allard, T., Vieira, L.C., Santos, R.V., Mancini, L., Seyler, P., 2015. Insights into iron sources and pathways in the Amazon River provided by isotopic and spectroscopic studies. Geochimica et Cosmochimica Acta 150, 142–159. https://doi.org/https://doi.org/10.1016/j.gca.2014.12.004

Oleinikova, O. V., Drozdova, O.Y., Lapitskiy, S.A., Demin, V. V., Bychkov, A.Y., Pokrovsky, O.S., 2017a. Dissolved organic matter degradation by sunlight coagulates organo-mineral colloids and produces low-molecular weight fraction of metals in boreal humic waters. Geochimica et Cosmochimica Acta 211, 97–114. https://doi.org/10.1016/j.gca.2017.05.023

Oleinikova, O. V., Poitrasson, F., Drozdova, O.Y., Shirokova, L.S., Lapitskiy, S.A., Pokrovsky, O.S., 2019. Iron isotope fractionation during bio- And photodegradation of organoferric colloids in boreal humic waters. Environmental Science and Technology 53, 11183−11194. https://doi.org/10.1021/acs.est.9b02797

Oleinikova, O. V., Shirokova, L.S., Gérard, E., Drozdova, O.Y., Lapitskiy, S.A., Bychkov, A.Y., Pokrovsky, O.S., 2017b. Transformation of organo-ferric peat colloids by a heterotrophic bacterium. Geochimica et Cosmochimica Acta 205, 313–330. https://doi.org/10.1016/j.gca.2017.02.029

Poitrasson, F., Vieira, L.C., Seyler, P., Pinheiro, G.M.D., Mulholland, D.S., Bonnet, M.P., Martinez, J.M., Lima, B.A., Boaventura, G.R., Chmeleff, J., Dantas, E.L., Guyot, J.L., Mancini, L., Pimentel, M.M., Santos, R.V., Sondag, F., Vauchel, P., 2014. Iron isotope composition of the bulk waters and sediments from the Amazon River Basin. Chemical Geology 377, 1–11. https://doi.org/10.1016/j.chemgeo.2014.03.019

Pokrovsky, O.S., Dupré, B., Schott, J., 2005. Fe-Al-organic colloids control of trace elements in peat soil solutions: Results of ultrafiltration and dialysis. Aquatic Geochemistry 11, 241–278. https://doi.org/10.1007/s10498-004-4765-2

Pokrovsky, O.S., Karlsson, J., Giesler, R., 2018. Freeze-thaw cycles of Arctic thaw ponds remove colloidal metals and generate low-molecular-weight organic matter 137, 321–336. Biogeochemistry. https://doi.org/10.1007/s10533-018-0421-6

Pokrovsky, O.S., Schott, J., 2002. Iron colloids/organic matter associated transport of major and trace elements in small boreal rivers and their estuaries (NW Russia). Chemical Geology 190, 141–179. https://doi.org/10.1016/S0009-2541(02)00115-8

Richter, F.M., Mendybaev, R.A., Christensen, J.N., Hutcheon, I.D., Williams, R.W., Sturchio, N.C., Beloso, A.D., 2006. Kinetic isotopic fractionation during diffusion of ionic species in water. Geochimica et Cosmochimica Acta 70, 277–289. https://doi.org/10.1016/j.gca.2005.09.016

Rodushkin, I., Stenberg, A., Andrén, H., Malinovsky, D., Baxter, D.C., 2004. Isotopic Fractionation during Diffusion of Transition Metal Ions in Solution. Analytical Chemistry 76, 2148–2151. https://doi.org/10.1021/ac035296g

Skulan, J., Beard, B., Johnson, C., 2002. Kinetic and equilibrium Fe isotope fractionation between aqueous Fe (III) and hematite. Geochimica et Cosmochimica Acta 66, 2995–3015. https://doi.org/10.1016/S0016-7037(03)00266-7

Swanner, E.D., Bayer, T., Wu, W., Hao, L., Obst, M., Sundman, A., Byrne, J.M., Michel, F.M., Kleinhanns, I.C., Kappler, A., 2017. Iron isotope fractionation during Fe (II)

oxidation mediated by the oxygen-producing marine cyanobacterium Synechococcus PCC 7002. Environmental science & technology 51, 4897–4906.

Swanner, E.D., Wu, W., Schoenberg, R., Byrne, J., Michel, F.M., Pan, Y., Kappler, A., 2015. Fractionation of Fe isotopes during Fe(II) oxidation by a marine photoferrotroph is controlled by the formation of organic Fe-complexes and colloidal Fe fractions. Geochimica et Cosmochimica Acta 165, 44–61. https://doi.org/https://doi.org/10.1016/j.gca.2015.05.024

Vasyukova, E. V., Pokrovsky, O.S., Viers, J., Oliva, P., Dupré, B., Martin, F., Candaudap, F., 2010. Trace elements in organic- and iron-rich surficial fluids of the boreal zone: Assessing colloidal forms via dialysis and ultrafiltration. Geochimica et Cosmochimica Acta 74, 449–468. https://doi.org/10.1016/j.gca.2009.10.026

Wu, J., Boyle, E., Sunda, W., Wen, L.S., 2001. Soluble and colloidal iron in the oligotrophic North Atlantic and North Pacific. Science 293, 847–849. https://doi.org/10.1126/science.1059251

Wu, L., Druschel, G., Findlay, A., Beard, B.L., Johnson, C.M., 2012. Experimental determination of iron isotope fractionations among Feaq2+–FeSaq–Mackinawite at low temperatures: Implications for the rock record. Geochimica et Cosmochimica Acta 89, 46–61. https://doi.org/https://doi.org/10.1016/j.gca.2012.04.047

Fig. 1. Temporal evolution of the (a) Fe % and (b) δ^{56}Fe in the < 30 kDa fractions for the low (black) and high (blue) Fe experiments at pH 1. The gray and blue zones correspond to δ^{56}Fe average of the initial solutions.

Fig. 2. Temporal evolution of the (a) Fe (black) and DOC (yellow) concentrations, (b) δ^{56}Fe, and (c) Fe % (black) and DOC % (yellow) in the < 30 kDa fractions for the experiment with OM at pH 6.5. The gray zone corresponds to δ^{56}Fe average of the initial solution.

Table 1 Iron isotopic composition, concentration, molar proportion in the < 30kDa fractions, and the initial solutions and real proportion of Fe precipitated in the >30kDa fractions (from different ultrafiltration units) for the low Fe concentration experiment at pH 1 and 6.5.

pH 1						
Time (min)	**V (mL)**	**Fe (µmol L^{-1})**	**$Fe_{<30kDa}$/ Fe_{tot} (mol./mol.) × 100 (%)**	**$Fe_{real\ precipitated}$ (mol./mol.) (%)**	**δ^{56}Fe ±2SD (‰)**	**δ^{56}Fe' ±2SD (‰)**
Initial	60 ± 1	85 ± 4	100		0.60 ± 0.13	
3	49 ± 5	84 ± 4	80 ± 10	1.8 ± 0.1	0.62 ± 0.13	0.03 ± 0.18
4	57 ± 5	79 ± 4	87 ± 10	7.5 ± 0.1	0.56 ± 0.13	-0.04 ± 0.18
5	54 ± 14	81 ± 4	85 ± 23	4.8 ± 0.3	0.56 ± 0.13	-0.04 ± 0.18
6	55 ± 21	81 ± 4	88 ± 33	4.6 ± 0.5	0.59 ± 0.14	-0.01 ± 0.19
7	57 ± 9	79 ± 4	89 ± 15	6.7 ± 0.2	0.62 ± 0.13	0.02 ± 0.18

10	51 ± 6	79 ± 4	79 ± 11	6.0 ± 0.2	0.54 ± 0.14	-0.06 ± 0.19

<LD: below limit of detection. nd: not determined.

Table 2 Iron isotopic composition, concentration, molar proportion in the < 30kDa fractions and the initial solutions, and real proportion of Fe precipitated in the >30kDa fractions (from different ultrafiltration units) for the high Fe concentration experiment at pH 1 and 6.5.

pH 1						
Time (min)	**V (mL)**	**Fe (mmol L^{-1})**	**$Fe_{<30kDa}$/ Fe_{tot} (mol/mol) × 100 (%)**	**Fe $_{real\ precipitated}$ (mol./mol.)(%)**	**δ^{56}Fe ±2SD (‰)**	**δ^{56}Fe' ±2SD (‰)**
Initial	60 ± 1	2.5 ± 0.1	100		0.57 ± 0.13	
3	46 ± 5	2.4 ± 0.1	76 ± 9	0.4 ± 0.1	0.59 ± 0.32	0.02 ± 0.34
4	48 ± 4	2.3 ± 0.1	76 ± 8	3.5 ± 0.1	0.59 ± 0.13	0.02 ± 0.18
5	50 ± 1	2.3 ± 0.1	79 ± 6	4.4 ± 0.1	0.54 ± 0.09	-0.03 ± 0.16
6	48 ± 6	2.4 ± 0.1	77 ± 12	2.4 ± 0.2	0.59 ± 0.06	0.01 ± 0.14
7	57 ± 4	2.4 ± 0.1	91 ± 9	3.4 ± 0.1	0.63 ± 0.06	0.05 ± 0.14
10	55 ± 3	2.4 ± 0.1	90 ± 8	0.9 ± 0.1	0.59 ± 0.13	0.02 ± 0.19

<LD: below limit of detection. nd: not determined

Table 3 Iron isotopic composition, concentration and molar proportion in the < 30kDa fractions and the initial solutions, and real proportion of Fe precipitated in the >30kDa fractions (from different ultrafiltration units) for experiment with OM at pH 6.5.

Time (min)	**V (mL)**	**DOC (mmol L^{-1})**	**$DOC_{<30kDa}$ / DOC_{tot} (mol/mol) %**	**Fe (µmol L^{-1})**	**$Fe_{<30kDa}$ / Fe_{tot} (mol/mol) %**	**Fe $_{real\ precipitated}$ (mol./mol.) (%)**	**δ^{56}Fe ±2SD (‰)**	**δ^{56}Fe' ±2SD (‰)**
Initial	60 ± 1	4.17 ± 0.21	100	104 ± 5	100		0.54 ± 0.08	
3	33 ± 6	1.07 ± 0.05	14 ± 3	4.1 ± 0.2	2.2 ± 0.4	52.8 ± 0.1	0.77 ± 0.13	0.24 ± 0.16
4	38 ± 2	0.96 ± 0.05	14 ± 1	2.9 ± 0.1	1.7 ± 0.2	61.2 ± 0.1	0.76 ± 0.05	0.23 ± 0.10
5	39 ± 1	0.88	14 ± 1	2.3 ±	1.5 ± 0.1	63.9 ±	0.87 ±	0.33

		± 0.04		0.1		0.1	0.04	± 0.09
6	45 ± 1	0.90 ± 0.05	16 ± 1	2.6 ± 0.1	1.9 ± 0.1	73.8 ± 0.1	0.77 ± 0.14	0.24 ± 0.16
7	47 ± 2	0.89 ± 0.04	17 ± 1	2.7 ± 0.1	2.0 ± 0.2	76.2 ± 0.1	0.80 ± 0.09	0.27 ± 0.12
10	48 ± 8	0.85 ± 0.04	16 ± 3	2.2 ± 0.1	1.7 ± 0.3	78.4 ± 0.1	0.82 ± 0.06	0.29 ± 0.10

DOC: Dissolved organic carbon.

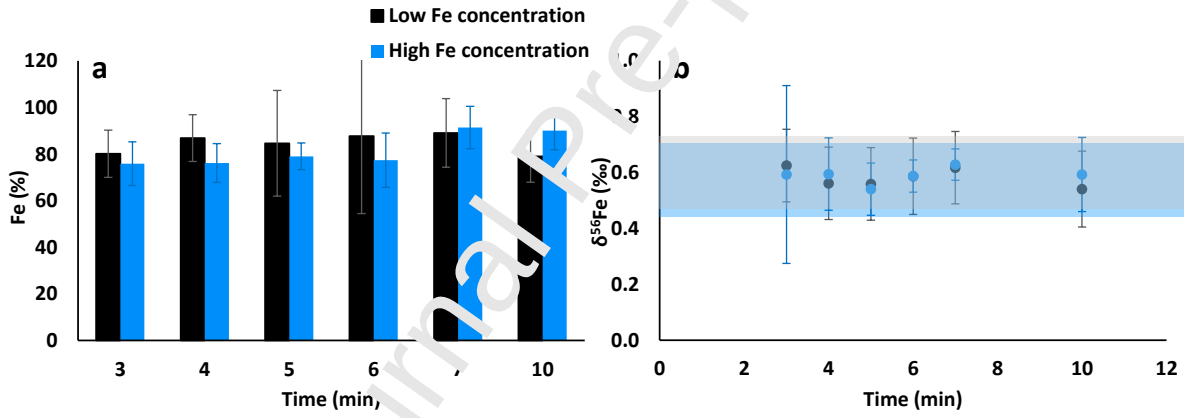

Figure 1

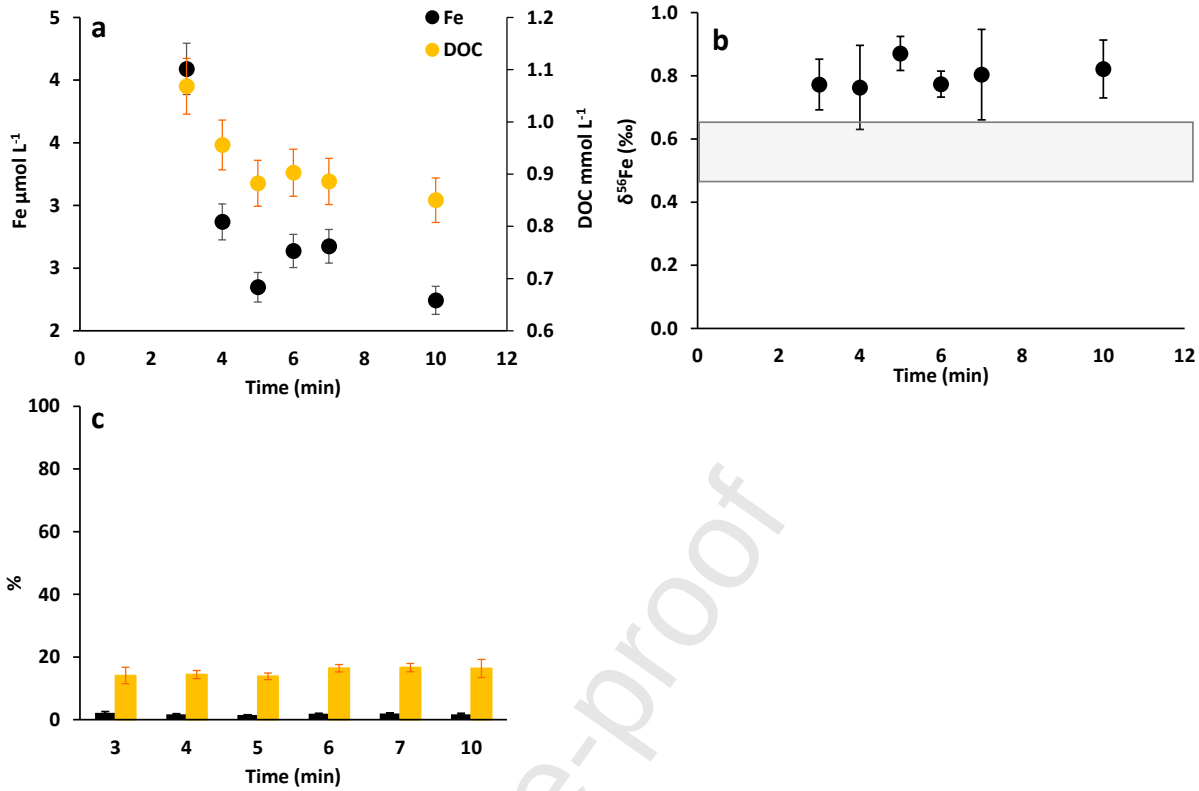

Figure 2